

Localization and delocalization properties in quasi-periodically-driven one-dimensional disordered systems

Hiroaki S. Yamada¹ and Kensuke S. Ikeda²

¹*Yamada Physics Research Laboratory, Aoyama 5-7-14-205, Niigata 950-2002, Japan*

²*College of Science and Engineering, Ritsumeikan University, Noji-higashi 1-1-1, Kusatsu 525-8577, Japan*



(Received 17 February 2022; accepted 11 April 2022; published 2 May 2022)

Localization and delocalization of quantum diffusion in a time-continuous one-dimensional Anderson model perturbed by the quasiperiodic harmonic oscillations of M colors is investigated systematically, which has been partly reported by a preliminary Letter [H. S. Yamada and K. S. Ikeda, *Phys. Rev. E* **103**, L040202 (2021)]. We investigate in detail the localization-delocalization characteristics of the model with respect to three parameters: the disorder strength W , the perturbation strength ϵ , and the number of colors, M , which plays the similar role of spatial dimension. In particular, attention is focused on the presence of localization-delocalization transition (LDT) and its critical properties. For $M \geq 3$ the LDT exists and a normal diffusion is recovered above a critical strength ϵ , and the characteristics of diffusion dynamics mimic the diffusion process predicted for the stochastically perturbed Anderson model even though M is not large. These results are compared with the results of discrete-time quantum maps, i.e., the Anderson map and the standard map. Further, the features of delocalized dynamics are discussed in comparison with a limit model which has no static disordered part.

DOI: [10.1103/PhysRevE.105.054201](https://doi.org/10.1103/PhysRevE.105.054201)

I. INTRODUCTION

It has been theoretically and experimentally shown that the three-dimensional random system undergoes an Anderson transition (AT) from insulator to metallic conductor due to decrease in the potential disorder [1–4]. Furthermore, in recent numerical experiments, the properties of AT in four-dimensional and five-dimensional random systems have been also studied [5–8]. In the system with the AT, a localization-delocalization transition (LDT) can exist, and its existence can be directly observed by the wave-packet dynamics of an initially localized wave packet, where the delocalization is observed as an appearance of normal diffusion.

In higher-dimensional Anderson models the appearance of delocalized states is quite natural, and it is expected that the self-consistent mean-field theory (SCT) works well in such systems [9,10]. However, even in higher-dimensional Anderson models the deviation of the critical value and the critical exponent predicted by the SCT was recently reported by using the properties of the energy spectrum [8].

The relationship between the dimension of the Anderson model and the characteristics of the LDT is an interesting problem from a different point of view. Increase of the system's dimension d may be performed in a quite different way: an alternative way to increase d is to make the system interact with many dynamical degrees of freedom. Indeed, even in the one-dimensional (1D) Anderson model exhibiting a strong exponential localization, the localization is released and normal diffusion is induced by the application of arbitrarily small stochastic perturbation, which can be considered as a superposition of an infinite number of incommensurate harmonic

degrees of freedoms [11–14]. This can be considered as a limiting example of delocalization realized in systems with infinite degrees of freedom.

Then it is a quite natural question to inquire how the number of the degrees of harmonic modes, M , controls the localization and delocalization in disordered systems. (The harmonic modes may be replaced the active phonon modes.) Indeed, in the case of chaotic quantum maps such as the standard map (SM), the harmonic perturbation destroys the dynamical localization and restores the chaotic diffusion [15–20], which is supported by the Maryland transformation asserting the equivalence between the SM and an $(M + 1)$ -dimensional lattice with a quasiperiodic disorder.

The quantum map is a very powerful model which can easily be treated by numerical methods because its time is discretized, but it is not a natural system. Instead, as a time-continuous model, we proposed a time-continuous 1D Anderson model interacting with M incommensurate harmonic modes [21,22]. For $M = 1$, the maintenance of localization can be shown by Floquet theory [23,24]. But for $M \geq 2$, diffusionlike behaviors are observed numerically at least on a finite time scale if the perturbation strength is strong enough. In this system, the M modes can be treated as quantum dynamical degrees of freedom, and so the whole system can be regarded as an autonomous quantum dynamical system with $M + 1$ degrees of freedom. There have been some studies showing a strong localized property of the dynamics for the same type of harmonically perturbed models. It is inferred from analytical calculation and rigorous proofs that the localization persists against the dynamical perturbation consisting of a finite number of modes [25,26].

In particular, the persistence of the localization for $1 \leq M < \infty$ is mathematically claimed in the regime of weak enough dynamical perturbations and strong disorder potential [26]. On the other hand, as mentioned above, a stochastic perturbation which corresponds to $M \rightarrow \infty$ can restore a complete diffusion. The presence of the LDT in a harmonically perturbed 1D Anderson model has not been yet clarified.

In our preliminary report it was shown that if there exist three or more harmonics ($M \geq 3$), the LDT occurs with the increase of the perturbation strength and the Anderson localized states can be delocalized [27]. This work is a full report of the localization-delocalization characteristics of the 1D Anderson model perturbed by polychromatic perturbations, which is numerically observed by changing three parameters: the disorder strength W , the perturbation strength ϵ , and the number of modes, M , of the oscillations. We are particularly interested in making clear how the number M controls the characteristics of the LDT. Additionally as a limiting situation of our model mentioned above, we can consider a model system without the static random potential (model B). Such a version leads to a quantum state that models the ultimate limit of delocalization exhibited by our model, which will be discussed in detail.

Since the direct numerical wave-packet propagation of the original continuous-time model is too time consuming, we proposed a discrete-time quantum map version of the original time-continuous model, which we called the Anderson map (AM), and investigated its nature in comparison with the SM and many-dimensional Anderson model [18–20]. Comparison of the original time-continuous model with the AM is also a purpose of this article.

Recently realization of an ergodic state in isolated quantum systems with many degrees of freedom has been extensively studied [28–32]. As mentioned above, our system is a closed quantum dynamical system with $M + 1$ degrees of freedom, and the LDT may be looked upon as a transition to an ergodic state even though M is small. The transition to a delocalized behavior is a “self-organization” of an irreversible relaxation process in quantum systems with a small number of degrees of freedom stressed in Ref. [33]. With this regard the minimal number of M above which the LDT takes place is a quite interesting problem.

The plan of the present work is as follows. In the next section, the models used in the present paper are introduced. In Sec. III, the characteristics of the localization phase which is dominant when the number M is small, i.e., $M = 0, 1, 2$, are explored. A hypothesis due to the intrinsic nature of the time-continuous model, which was not taken into account in our preliminary report [27], is discussed. In particular, in Sec. III E, we give a different interpretation from Ref. [27] for the color number M used as a base of the following analysis in the later sections. Next, in Sec. IV, the presence of LDT for the case of $M \geq 3$ is demonstrated and the characteristics of the LDT are clarified on the basis of the one-parameter scaling theory together with the above hypothesis. The presence of critical subdiffusion, the invariant nature of critical perturbation strength, and their dependency upon M are fully discussed. After these arguments, we reexamine the absence of LDT in the case of $M = 2$ in Sec. V. Finally, in Sec. VI,

the characteristics of the normal diffusion in the delocalized states are discussed in some detail, and compares with result in model B. A summary and discussion appear in the last section.

II. MODELS

We consider a one-dimensional tightly binding disordered system represented by the lattice site basis $|n\rangle$ (n integer) with the probability amplitude Ψ_n , which is driven by time-dependent quasiperiodic perturbation. The Schrödinger equation of the above system is represented by

$$i\hbar \frac{\partial \Psi_n(t)}{\partial t} = \Psi_{n-1}(t) + \Psi_{n+1}(t) + V(n, t)\Psi_n(t), \quad (1)$$

where $V(n, t)$ is the time-dependent on-site potential. We deal with the following two cases, $V_A(n, t)$ and $V_B(n, t)$, as $V(n, t)$ with coherent periodic perturbation $f_\epsilon(t)$:

$$V(n, t) = \begin{cases} V_A(n, t) = V(n)[1 + f_\epsilon(t)] & \text{(model A)} \\ V_B(n, t) = V(n)f_\epsilon(t) & \text{(model B)}. \end{cases} \quad (2)$$

The coherent periodic perturbation $f_\epsilon(t)$ is given as

$$f_\epsilon(t) = \frac{\epsilon}{\sqrt{M}} \sum_i^M \cos(\omega_i t + \theta_i), \quad (3)$$

where M and ϵ are the number of the frequency component and the relative strength of the perturbation, respectively. Note that the long-time average of the total power of the perturbation is normalized to $\overline{f_\epsilon(t)^2} = \epsilon^2/2$. The frequencies $\{\omega_i\}$ ($i = 1, \dots, M$) are taken as mutually incommensurate numbers of order $O(1)$ given in Appendix A. Here we take $\theta_i = 0$ ($i = 1, 2, \dots, M$) to see long-term results that do not depend on the details of initial phases $\{\theta_i\}$. The static on-site disorder potential is represented as $V(n) = Wv_n$. W denotes the strength of the potential, and v_n is a uniform random variable with the range $[-1, 1]$ which is decorrelated between different sites. In model A, it becomes the Anderson model if we take $\epsilon = 0$, and the Anderson localization occurs. How the localization may become delocalized by increasing the perturbation strength ϵ is the main problem to be clarified. On the other hand, model B is controlled by the combined parameter ϵW , and if we take $\epsilon W = 0$, the eigenstates are the Bloch states. The issue is how the ballistic motion of $\epsilon = 0$ may make the transition to a stochastic motion such as the normal diffusion by increasing ϵ , which models stochasticization of ballistic electrons by dynamical impurities.

We remark that time-dependent model (1) has an autonomous representation. The isolated harmonic modes form an M -dimensional ladder of the eigenstate $| \{n_i\} \rangle$ which is assigned by the set of integers $\{n_i\}$ ($1 \leq i \leq M$) as the quantum numbers and has the energy $E_h(\{n_i\}) := \sum_{i=1}^M \omega_i n_i$. If we denote the eigenstate of the 1D Anderson model of $\epsilon = 0$ by $|N\rangle$, which are the Anderson localized state (model A) or Bloch states (model B) having the energy eigenvalue E_N , then Eq. (1) is equivalent to the autonomous Schrödinger equation describing the transition process in an $(M + 1)$ -dimensional lattice of sites assigned by $(N, \{n_i\})$: let the probability amplitude of the quantum state $|N, \{n_i\}\rangle = |N\rangle | \{n_i\} \rangle$ be $\Phi(N, \{n_i\})$,

then the Schrödinger equation is represented by

$$i\hbar \frac{d\Phi(N, \{n_i\})}{dt} = [E_N + E_h(\{n_i\})]\Phi(N, \{n_i\}) + \frac{\epsilon}{\sqrt{M}} \sum_{N'} \sum_{j=1}^M W_{NN'} \Phi(N', n_1, \dots, n_j \pm 1, n_{j+1}, \dots, n_M), \quad (4)$$

where $W_{NN'}$ is the transition element $W \sum_n \langle N|n\rangle v_n \langle n|N'\rangle$ and $\{|n\rangle\}$ is an orthonormalized basis set representing the lattice site n . The equivalent of Eq. (4) to the autonomous version of Eq. (1) is presented in Appendix B.

We basically limit the perturbation strength to $\epsilon < 0.3$, since we are interested in how small ϵ may destroy the localization effect. As ϵ increases far beyond the perturbation regime, model A will gradually approach to model B.

As the tool of numerical integration of Eq. (1), we use the second-order symplectic integrator

$$U(\ell) = e^{-i\Delta t \cos(n)/2\hbar} e^{-iV(n, \ell \Delta t)/\hbar} e^{-i\Delta t \cos(n)/2\hbar} \quad (5)$$

with the small-enough time step $\Delta t = 0.02-0.05$, where the value of the Planck constant is taken as $\hbar = 1/8$. The system and ensemble sizes are $2^{15}-2^{16}$ and $10-50$, respectively, throughout this paper. We use a localized state at $n = n_0$ as the initial state and numerically observe the spread of the wave packet measured by the mean square displacement (MSD),

$$m_2(t) = \sum_n (n - n_0)^2 \langle |\Psi(n, t)|^2 \rangle. \quad (6)$$

In the limit $M \rightarrow \infty$, the quasiperiodic perturbation $f_\epsilon(t)$ can be identified with the δ -correlated stochastic force $n(t)$ characterized by $\langle n(t)n(t') \rangle = \epsilon_s^2 \delta(t - t')$ with the strength ϵ_s . In this paper, corresponding models A and B, we consider the stochastic version of the two models in which the harmonic force $f_\epsilon(t)$ is replaced by the noise force $n(t) = \epsilon_s n_1(t)$, which varies at random in time uniformly in the range $[-1, 1]$:

$$\begin{cases} V_{SA}(n, t) = V(n)[1 + \epsilon_s n_1(t)] & \text{(model SA)} \\ V_{SB}(n, t) = V(n)\epsilon_s n_1(t) & \text{(model SB)}. \end{cases} \quad (7)$$

We call these models SA and SB, respectively. In model SA, the localization is destroyed by the stochastic perturbation and the normal diffusion $m_2(t) = Dt$ with the diffusion constant D appears for $t \rightarrow \infty$ [21,22], as was first pointed out by Haken and co-workers [11,12]. They predicted analytically the diffusion constant D for the white Gaussian noise as

$$D = \lim_{t \rightarrow \infty} \frac{m_2(t)}{t} \propto \frac{\epsilon_s^2}{\epsilon_s^4 + W^2/3} \quad (8)$$

for weak enough ϵ_s . The diffusion constant increases as $D \propto \epsilon_s^2$ for $\epsilon_s \ll 1$ and it reaches a maximum at $\epsilon_s^* = \frac{W}{\sqrt{3}}$, and it finally decreases as $D \propto \epsilon_s^{-2}$. The noise-induced diffusion has been extended for a random lattice driven by the colored noise, including the hopping disorder effect [13,14].

For finite M , $f_\epsilon(t)$ can no longer be replaced by the random noise, and it plays as a coherent dynamical perturbation, and the system corresponds to a quantum dynamical system with $M + 1$ degrees of freedom.

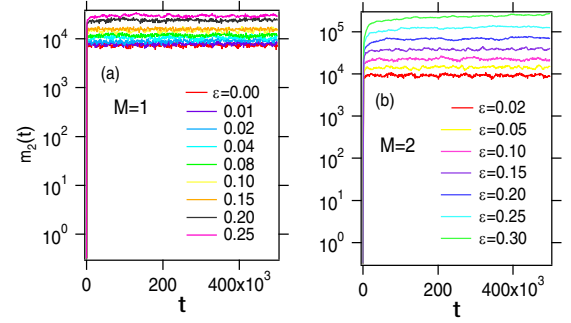


FIG. 1. The plots of $m_2(t)$ as a function of time for different values of ϵ increasing from bottom to top in the perturbed Anderson model: (a) $M = 1$, $W = 1.0$; (b) $M = 2$, $W = 1.0$. Note that the horizontal axes are in the logarithmic scale.

III. LOCALIZED STATES OF MODEL A

First of all we show in this section the localization characteristics exhibited by our model in Eq. (1). The cases of $M = 1, 2$ are particularly focused on, and a basic hypothesis to interpret all our numerical results is discussed in connection with the localization characteristics of our system.

A. Dynamics toward localization, localizing evolution

Figure 1(a) shows the time dependence of the MSD for some typical cases of the monochromatically perturbed model A, for which the growth of time dependence is saturated at a certain level. The spread of the wave packet becomes larger as the perturbation strength increases. This is the same tendency as was observed for the Anderson map. In this paper, we directly compute the localization length (LL) by

$$\xi_M = \sqrt{m_2(\infty)}, \quad (9)$$

where $m_2(\infty)$ indicates the numerically saturated MSD reached after a sufficiently long time evolution. For $M = 1$ the localization is manifest. Even in the case of $M = 2$, localization occurs and the LL increases as the perturbation strength increases, as can be seen from Fig. 1(b).

Application of harmonic perturbation in general enhances the LL. The enhancement of LL is conspicuous for $M = 2$, and the numerical evaluation of ξ_M directly from the long time behavior of MSD is possible only in the limited range of $\epsilon < 0.4$.

B. W dependence of localization length

Figure 2 shows the W dependence of the LL ξ_M for $M = 0, 1, 2$. In all cases, it is naturally found that for $\epsilon \ll 1$ the larger W , the stronger the localization is, and the LL follows the rule

$$\xi_M \sim \frac{A_M(\epsilon)}{W^2}, \quad (10)$$

where $A_M(\epsilon)$ depends on M and ϵ . The W^{-2} dependence of the LL has been commonly observed in the case of quantum map systems [20]. For $M = 1$ the persistence of localization can be expected as is argued in Appendix C.

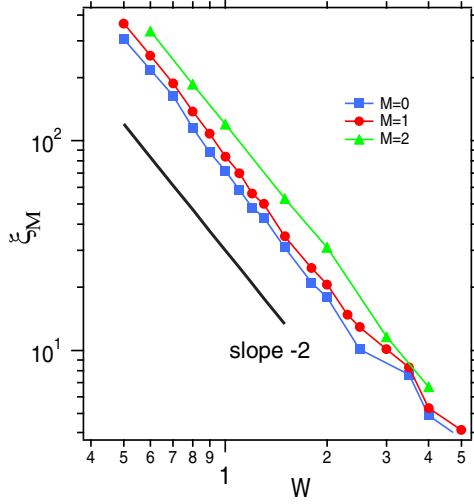


FIG. 2. Localization length ξ_M of model A as a function of disorder strength W for $M = 0, 1, 2$ and $\epsilon = 0.05$.

C. ϵ dependence of localization length ($\epsilon \ll 1$)

Figure 3(a) shows the result of the ϵ dependence in model A of $M = 1, 2$ for some W 's. It is obvious that the LL grows exponentially as the perturbation strength ϵ increases in all cases:

$$\xi_M \sim e^{c_M \epsilon}. \quad (11)$$

When W is the same, the exponential growth rate c_M of $M = 2$ is larger than that of $M = 1$, and it can be seen that the coefficient c_M does not depend on the disorder strength W . To confirm this more concretely, we plot the ϵ dependence in Fig. 3(b) of the scaled LL $\xi \times W^2$. At least when ϵ is small ($\epsilon < 0.3$), they all overlap well, and the coefficient c_M is almost constant and has no W dependence. Therefore,

$$\xi_M \simeq \frac{\exp\{c_M \epsilon\}}{W^2}. \quad (12)$$

This is similar to what was found for the monochromatically perturbed Anderson map [19] in a small region of ϵ .

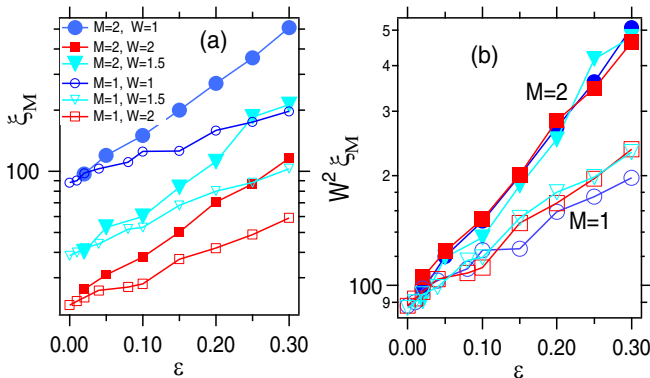


FIG. 3. (a) Localization length ξ_M of model A as a function of perturbation strength ϵ for $M = 1, 2$ and $W = 1.0, 1.5, 2.0$. (b) $\xi_M W^2$ as a function of ϵ . Note that the vertical axes are in logarithmic scale.

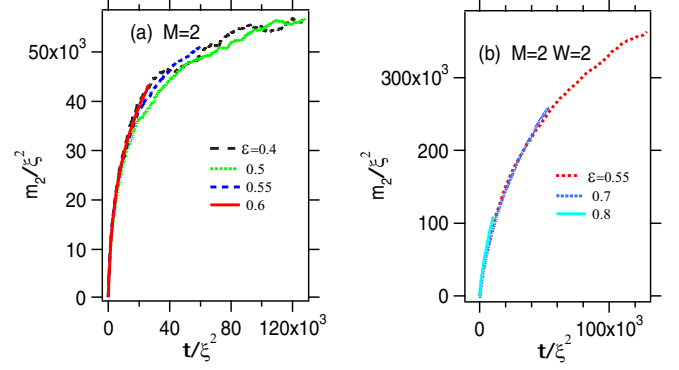


FIG. 4. Scaling property $m_2(t)/\xi(\epsilon)^2$ as a function of $t/\xi(\epsilon)^2$ in the dichromatically perturbed model A of $W = 1$ for various ϵ 's. (a) $\epsilon = 0.40, 0.50, 0.55, 0.60$ and (b) $\epsilon = 0.55, 0.70, 0.80$.

Although it is difficult to obtain the LL ξ_M directly from the long time behavior of MSD, it can be expected that a similar tendency to the cases of $M = 1$ and $M = 2$ will be observed even in the localized region of $M \geq 3$ for small enough ϵ . However, as is the case in the high-dimensional disordered lattices and also in the Anderson map system, if LDT takes place at some critical ϵ_c , the LL grows divergently as $\epsilon \rightarrow \epsilon_c$.

D. ϵ dependence of localization length for large ϵ

We observed that, at least, the wave packet localizes completely when $M = 2$ in the region where the perturbation strength is relatively small, $\epsilon < 0.4$. We would like to investigate the localization length ξ_M for $M = 1$ and $M = 2$ when ϵ increases beyond the perturbation region. In the region where ϵ is large, the localization length ξ_M cannot be estimated directly by the saturation level of the MSD.

Here, we try to determine ξ_M indirectly by supposing that the MSD data follow the common scaling form independent of ϵ as

$$m_2(t) \sim \xi(\epsilon)^2 F\left(\frac{t}{\xi(\epsilon)^2}\right), \quad (13)$$

where $F(x)$ is a scaling function. To confirm this, we show in Fig. 4 the plots of $m_2/\xi(\epsilon)^2$ as a function of $t/\xi(\epsilon)^2$, which manifests the scaling hypothesis of Eq. (13).

We can estimate the localization length $\xi_M(\epsilon)$ by using, and sometimes by repeatedly using, the scaling hypothesis of Eq. (13) even for $\epsilon > 0.4$.

Figure 5 shows the ϵ dependence of a wide range of the localization lengths, including indirectly determined ξ_M with the scaling hypothesis (13). For comparison, ξ_M of $M = 3$, which exhibits a clear LDT as discussed in detail later, is also shown. The localization, of course, occurs in the case of $M = 1$.

Then what is the difference of the localizations between the case of $M = 1$ and the cases of $M = 2$? In both cases of $M = 1$ and $M = 2$, the localization lengths grow exponentially when the ϵ is small enough ($\epsilon < 0.8$ for $M = 1$ and $\epsilon < 0.3$ for $M = 2$).

For $M = 1$, it is obvious that the localization occurs no matter how large ϵ may be, but, as for $M = 2$, the presence or absence of LDT is still unclear. We will discuss again the

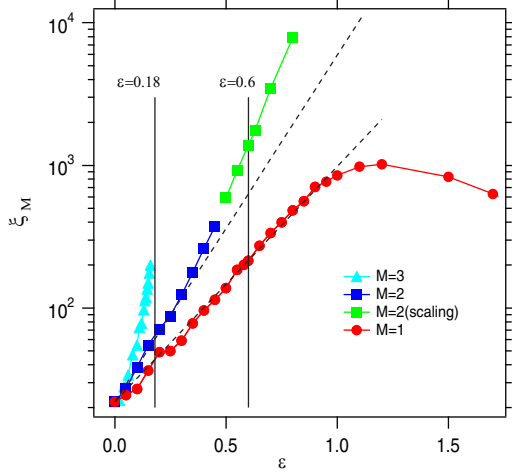


FIG. 5. Localization length as a function of ϵ for $M = 1, 2, 3$ with $W = 1$. Some LLs of $M = 2$ are obtained by the scaling hypothesis of Eq. (13) for $\epsilon > 0.4$. Note that the horizontal axis is in logarithmic scale. The dashed lines are $e^{5.5\epsilon}$ and $e^{3.8\epsilon}$, respectively. The lines $\epsilon = 0.18$ and $\epsilon = 0.6$ are shown as a reference.

persistence of localization for $M = 2$ in Sec. V after Sec. IV, in which the presence of LDT is confirmed for $M \geq 3$. In the next section we consider the *substantial dimension* of our system which may dominate the upper-bound dimension of localization.

E. The effective dimension

Our model (1) is very similar to that of the AM perturbed by M harmonic modes, which is represented by the symplectic propagator (5) of $\Delta t = 1$. It is formally transformed into a $d (= M + 1)$ -dimensional quasirandom lattice by the so-called Maryland transformation [20], and $d = 2$, i.e., $M = 1$, is the upper bound of dimension in which delocalization does not happen. Unlike this, in the present model the numerical observations suggest $M = 2$ may be the upper-bound dimension of the localization. Why is there such a difference?

In the case of the AM, time is not continuous and there is no conserved quantity. However, in the present case, Eq. (1) is rewritten as Eq. (B3) given in Appendix B, which yields a severe constraint of energy conservation. In the transition process by the interaction among the harmonic modes and the isolated 1D random lattice the constraint due to the energy conservation,

$$\left| \sum_{m=1}^M \Delta n_m \omega_m \right| < \frac{|E_N - E_{N'}|}{\hbar} < \frac{C}{\hbar}, \quad (14)$$

exists, where E_N and $E_{N'}$ are the energies of the localized eigenstates and $\Delta n_i = n'_i - n_i$ is the change of excitation number of the i th harmonic mode. The upper bound of $C = \text{Max}\{|E_N - E_{N'}|\}$ is estimated as $C < 4 + 2W$. If $C = 0$, the number of degrees of freedom reduces by exactly 1, and

$$d_f = (M - 1) + 1 = M \quad (15)$$

is the effective dimension of the system. However, since C is finite, the system should be regarded as the “quasi- d_f ”-dimensional system in the sense that $M - 1$ quantum numbers

can arbitrarily be changed but the M th mode is restricted by Eq. (14). If d_f corresponds to the spatial dimension of the irregular lattice, then the maximal dimension in which only the localization exists can be $d_f = M = 2$ if the scaling theory of the localization is followed. In the present paper we interpret the results presented below on the hypothesis that Eq. (15) is the “effective dimension.” We emphasize that the hypothesis was not taken into account in our previous Letter, and $M + 1$, instead of $M = d_f$, was used as the system dimension [27].

IV. LOCALIZATION-DELOCALIZATION TRANSITION: MODEL A

In this section, we investigate the LDT of model A with increasing the number of colors from $M = 3$ to $M = 7$ while paying attention to the correspondence with result in the Anderson map system. The case of $M = 2$, which has a large localization length but is expected to have no LDT, will be discussed again in the next section.

A. Dynamical LDT

In Fig. 6, typical examples indicating the LDT for $M \geq 3$ are depicted. They are the double logarithmic plot of the time evolution of MSD for an increasing series of the perturbation strength ϵ . For both examples one can recognize that with an increase in ϵ the time evolution of MSD exhibits a transition from a saturating behavior to a straight line of slope 1 implying the normal diffusion $m_2 \propto t$. A remarkable fact is that the transition proceeds through a time evolution represented by a straight increase with a fractional slope $0 < \alpha < 1$ at a particular value $\epsilon = \epsilon_c$. It can be regarded as the critical subdiffusion $m_2 \propto t^\alpha$. Indeed, for $M \geq 3$ the numerical results indicate that the asymptotic behavior of the MSD in the limit $t \rightarrow \infty$ changes as

$$m_2(t) \sim \begin{cases} t^0 \text{ (localization)}, & \epsilon < \epsilon_c \\ t^\alpha \text{ (subdiffusion)}, & \epsilon \simeq \epsilon_c \\ t^1 \text{ (delocalization)}, & \epsilon > \epsilon_c, \end{cases} \quad (16)$$

which fully follows the numerical observations in the AM and SM [20].

To confirm numerically the critical behavior represented by Eqs. (16), it is very convenient to introduce the local diffusion exponent defined as the instantaneous slope of the log-log plot of MSD,

$$\alpha_{\text{ins}}(t) = \frac{d \log m_2(t)}{d \log t}, \quad (17)$$

as a function of t , where $m_2(t)$ is appropriately smoothed.

Figures 6(a)–6(c) and 6(d)–6(f) are examples of the transition process modeled by Eqs. (16) for $M = 3$ and $M = 5$, respectively. Figures 6(a) and 6(d) represent the change of MSD from the localized states to the normal diffusion state. Transition from the localized state to the normal diffusion is directly recognized by the change of $\alpha_{\text{ins}}(t)$ plots demonstrated in Figs. 6(b) and 6(e). It either decays to zero or increases toward 1, and it keeps a constant value only at a particular $\epsilon = \epsilon_c$, indicated by broken lines, which means the existence of the critical subdiffusion $m_2(t) \propto t^{\alpha_c}$ at $\epsilon = \epsilon_c$,

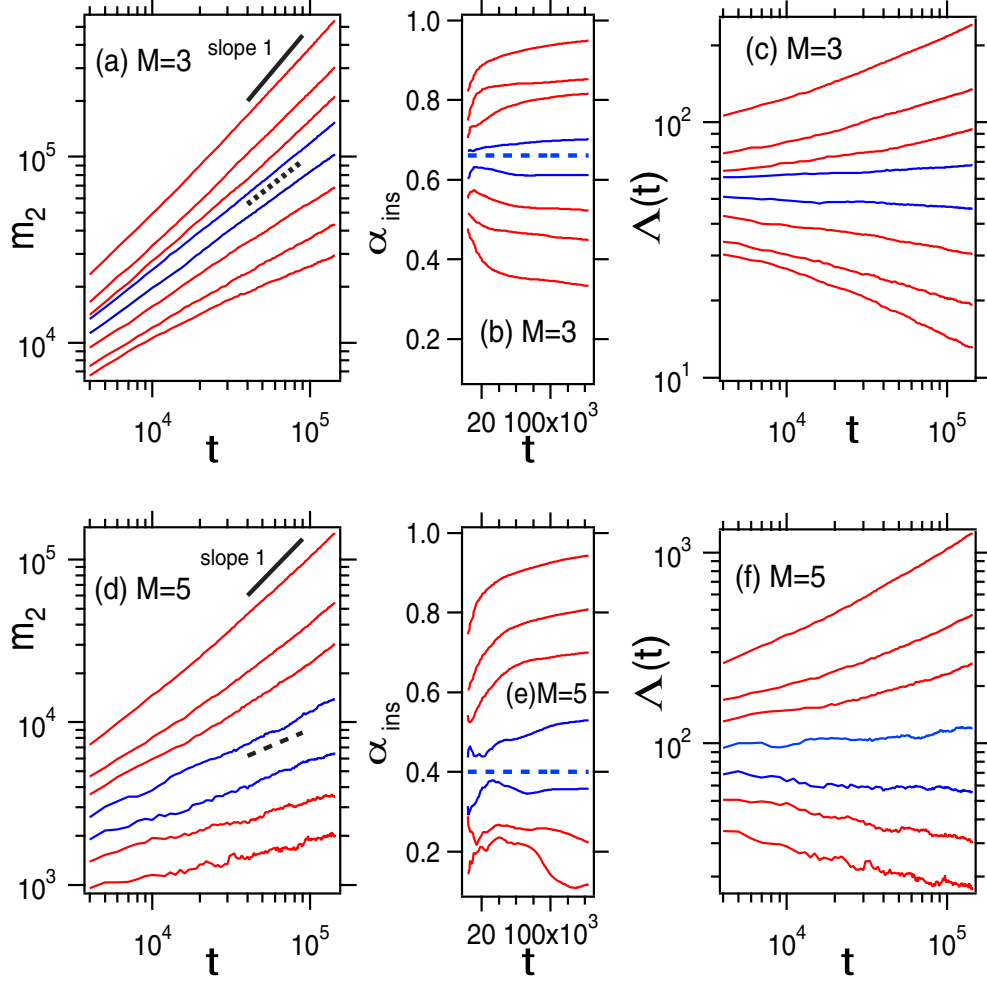


FIG. 6. Localization-delocalization transition for model A exhibited by the change of time dependence of MSD: (a-c) $M = 3$ and $W = 1$ and (d-f) $M = 5$ and the same $W = 1$. (a) The double-logarithmic plots of MSD $m_2(t)$, (b) the diffusion index $\alpha_{\text{ins}}(t)$, and (c) the scaled MSD $\Lambda(\epsilon, t) = m_2(t)/t^{\alpha_c}$, where $\alpha_c = 0.66$, as functions of time for increasing perturbation strengths $\epsilon = 0.17, 0.18, 0.19, 0.20, 0.21, 0.22, 0.23, 0.25$ from below. The broken line in (b) indicates the critical subdiffusion line $\alpha_{\text{ins}}(t) = \alpha_c = 0.66$ predicted by the scaling theory. Plots (d-f) are the counterparts of (a-c), respectively, for $M = 5$, where ϵ is increased as $\epsilon = 0.05, 0.06, 0.07, 0.08, 0.09, 0.10, 0.12$ from below and $\alpha_c = 0.40$.

where $0.60 < \alpha_c < 0.70$ and $0.35 < \alpha_c < 0.45$ in Figs. 6(b) and 6(e), respectively.

These facts suggest the so-called one-parameter scaling theory, which was successfully used in the analyses of AM and SM, is applicable to our model, identifying the effective dimension in Eq. (15) as the dimension d of the random system. It predicts the critical subdiffusion index as

$$\alpha = \frac{2}{d_f} = \frac{2}{M}. \quad (18)$$

The theoretical value $\alpha \sim 0.66$ for $M = 3$ and $\alpha \sim 0.40$ for $M = 5$ are drawn in Figs. 6(b) and 6(e) by broken lines, respectively. Agreement with the critical lines suggested by $\alpha_{\text{ins}}(t)$ plots is evident. We note that in our preliminary report we took $d_f = M + 1$, instead of Eq. (15), because the restriction (14) was not taken into account. However, as M increases beyond 5, Eq. (18) become less confirmative.

To make a further check of the LDT close to the critical point, it is instructive to use the MSD $\Lambda(t)$ divided by the

critical subdiffusive increase:

$$\Lambda(t) \equiv \frac{m_2(t)}{t^{\frac{2}{M}}}. \quad (19)$$

Then $\Lambda(t) \simeq \text{const}$ indicates the critical point, and $\Lambda(t)$ grows upward for $\epsilon > \epsilon_c$, while it decays downward for $\epsilon < \epsilon_c$, as seen in Figs. 6(c) and 6(f). The feature for which the $\Lambda(t)$ curves expands like a trumpet-shaped suggests the existence of the LDT.

As shown in Fig. 7, we confirm that the critical subdiffusion can be observed at certain critical point $\epsilon = \epsilon_c$ even if M is increased beyond 3, and it is evident that the subdiffusion index α at the critical point decreases as M increases, and it is numerically consistent with the prediction of Eq. (18).

B. M dependence of the scaling property for the LDT

In Fig. 8(a), we show result of finite-time scaling analysis for model A of $M = 3$. The method used here is the same as that used in Ref. [20]. We choose the following quantity as a

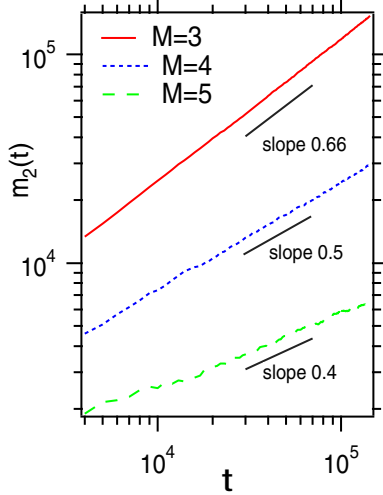


FIG. 7. The double-logarithmic plots of $m_2(t)$ as a function of time near the critical points ϵ_c in the polychromatically perturbed 1D Anderson model ($M = 3, 4, 5$ from top) with $W = 1$.

scaling variable,

$$\Lambda_s(\epsilon, t) = \log \Lambda(\epsilon, t) = F(x), \quad (20)$$

by shifting the time axis to x ,

$$x = \xi_M(\epsilon)t^{\alpha/2\nu}, \quad (21)$$

for different values of ϵ by using the critical exponent ν to characterize the divergence of the localization length around

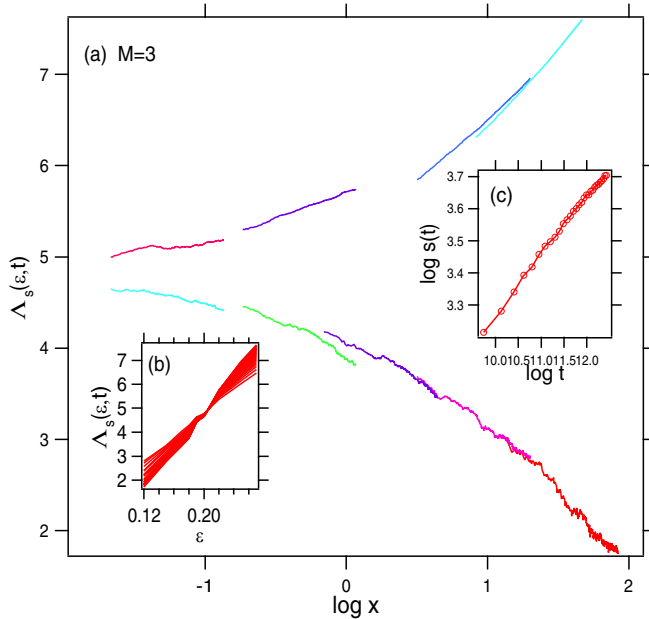


FIG. 8. The results of the critical scaling analysis for trichromatically perturbed model A ($M = 3$) with $W = 1.0$. (a) The scaled MSD $\Lambda_s(\epsilon, t) = \log \Lambda(\epsilon, t)$ as a function of $x = \xi_M(\epsilon)t^{\alpha/2\nu}$ for some values of ϵ . (b) The scaled $\Lambda_s(\epsilon, t)$ with $\alpha = 0.66$ as a function of ϵ for some pickup times. The crossing point is $\epsilon_c \simeq 0.21$. (c) $s(t)$ as a function of t . The critical exponent $\nu \simeq 1.81$ is determined by a scaling relation [Eq. (23)] by the least-squares fit.

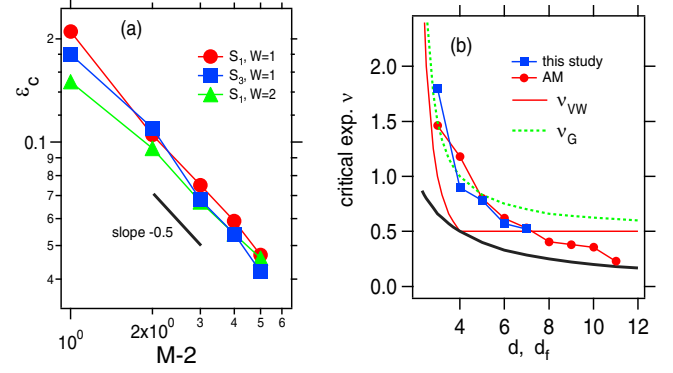


FIG. 9. (a) The critical perturbation strength ϵ_c as a function of $M - 2$ for model A with $W = 1$. The black solid line shows $\epsilon_c \propto 1/(M - 2)^{0.5}$. (b) The effective dimensionality $d_f = M$ dependence of the critical exponent ν which characterizes the critical dynamics. The red solid line and green dashed line are the results of the analytical prediction by ν_{VW} and ν_G , respectively. The thick line denotes the lower bound by the Harris critical inequality.

the LDT:

$$\xi_M \sim |\epsilon - \epsilon_c|^{-\nu}. \quad (22)$$

$F(x)$ is a differentiable scaling function and α is the diffusion index.

Figure 8(b) shows a plot of $\Lambda_s(t)$ as a function of ϵ at several times t , and it can be seen that this intersects at the critical point ϵ_c . In addition, Fig. 8(c) shows a plot of

$$s(t) = \frac{\Lambda_s(\epsilon, t) - \Lambda_s(\epsilon_c, t)}{|\epsilon_c - \epsilon|} \propto t^{\alpha/2\nu} \quad (23)$$

as a function of t , and the critical localization exponent ν is determined by best fitting this slope. This is consistent with formation of the one-parameter scaling theory (OPST) of the localization. As a result, even in model A, the OPST is well established for the LDT regardless of the number of colors, M , and the disorder strength W .

The critical exponent evaluated using the data ($\alpha = 0.66$, $\epsilon_c = 0.21$) at $W = 1$ for $M = 3$ is $\nu \simeq 1.81$. The same is true for the other $M (\geq 4)$ color perturbations. Appendix D shows the results of the finite-time scaling analysis when $M = 4$ and $M = 7$. These results are similar to that of the AM system perturbed by the $M - 1$ colors and of numerical calculations using finite-size scaling in the $d_f (= M)$ -dimensional random systems. Note that pursuing the numerical value of ν with high accuracy is not the purpose of this paper.

C. M dependence of critical strength ϵ_c

We return to the story of critical perturbation strength ϵ_c . As is seen in Fig. 9(a), ϵ_c definitely decreases with increase in M for $M \geq 3$. Looking upon ϵ_c as the function of $M - 2$, the double-logarithmic plots are on a straight line with the approximate tangent -0.5 , namely,

$$\epsilon_c \sim \frac{1}{(M - 2)^\delta}, \quad \delta \simeq 0.5. \quad (24)$$

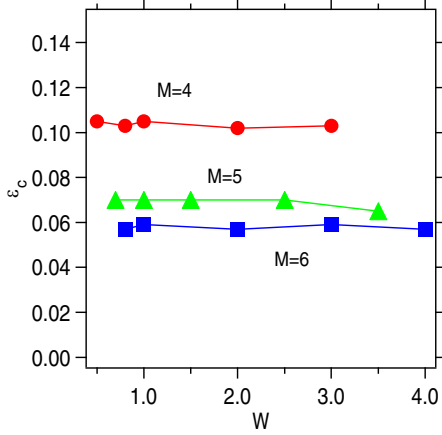


FIG. 10. The critical perturbation strength ϵ_c as a function of W in model A of $M = 4, 5, 6$ (from top).

This result suggests that ϵ_c diverges at $M = 2$, and the LDL transition does not exist at $M = 2$. Evident dependence of ϵ_c on M for large M contradicts the prediction of the SCT [20].

The critical exponent ν , which characterizes the divergence of the localization length at the critical point, is numerically evaluated, and plotted against M , as shown in Fig. 9(b). As a result, it can be seen that the tendency for $M \geq 3$ is close to that in the Anderson map.

D. W dependence of the critical point ϵ_c

Figure 10 shows the W dependence of the critical perturbation strength ϵ_c for $M = 4, M = 5$, and $M = 6$. From this result, it can be inferred that the critical perturbation strength ϵ_c of the LDT keeps an almost constant value insensitive to the disorder strength W and is only determined by the number of colors, M . Such a feature agrees with that observed in the Anderson map system with $M \geq 2$ for which the LDT emerges. We show another direct evidence manifesting that the magnitude of W does not influence the LDT. The time evolution of the MSD at ϵ_c is shown for several values of W in Fig. 11. First, looking at the case of $M = 4$ in Fig. 11(a), the spread $m_2(t)$ of the wave packet becomes larger with decrease in W , as is expected. But in all cases we see that for the same $\epsilon = \epsilon_c = 0.115$ a subdiffusive increase at the same index $\alpha \simeq 0.5$ emerges regardless of W . Similarly, in the case of $M = 6$, regardless of W , for the same $\epsilon_c \simeq 0.058$ the subdiffusion of $\alpha \simeq 0.33$ emerges, as seen in Fig. 11(c).

Figures 11(b) and 11(d) are the enlargement of the initial growth of MSD for $t < 10^2$ of Figs. 11(a) and 11(c), respectively. In all cases, the wave packet starts with a ballistic expansion $m_2 \sim t^2$ and changes to exhibit the critical subdiffusion after a lapse of characteristic time. A paradoxical fact is that the characteristic time required for realizing the subdiffusive delocalization decreases with increase in the disorder strength W .

The larger the W , the stronger the localization, and as the localization becomes stronger, delocalization occurs more promptly. This means that what is important for delocalization is not to activate the ballistic expansion of the wave packet, but to promote its decomposition into particlelike quantum states

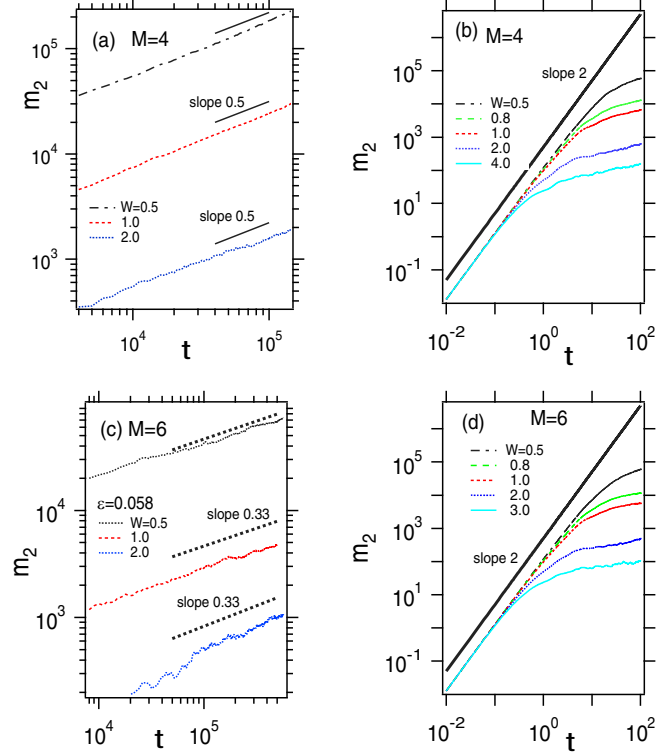


FIG. 11. The double-logarithmic plots of $m_2(t)$ as a function of time t near the critical points ϵ_c for different W in model A of (a) $M = 4$ and (c) $M = 6$. Panels (b) and (d) show the enlarged view of the short-time region $t < 10^2$ in the double-logarithmic plots of $m_2(t)$ in model A of (b) $M = 4$ and (d) $M = 6$.

called localized states due to the accumulation of scattering by disorder. Delocalization emerges as the diffusive motion over the localized particlelike states.

V. RECONSIDERATION OF WEAK DYNAMICAL LOCALIZATION FOR $M = 2$

We return to the problem on the presence of LDT in the case of $M = 2$. It is very hard to numerically prove the persistence of localization, either by directly pursuing time evolution dynamics or by applying the scaling hypothesis [see Fig. 12(a)]. However, there are some evidences manifesting that there exists no critical subdiffusion such that $m_2 \propto t^\alpha$ with $0 < \alpha < 1$. To numerically prove the presence of critical subdiffusion, an explicit method is to use the $\alpha_{\text{ins}}(t)$ plots presented in the previous section. We examine in Fig. 12(b) the $\alpha_{\text{ins}}(t)$ plots for $M = 2$. All the curves go downward and it can hardly be expected that a horizontal line locates in the narrow gap between the line $\alpha = 1$ and the uppermost downward curve, which implies that $\alpha = 1$ plays the role of “critical diffusion.” This fact is consistent with the results of the previous section represented by Eqs. (18) and (24) for $M \geq 3$, which predict $\alpha = 1$ and $\epsilon_c = \infty$, respectively, for $M = 2$.

We further examine in Fig. 12(c) the Λ plots of Eq. (19), namely, the MSD scaled by the critical MSD $m_2(t) \propto t^\alpha$, which is $\Lambda(\alpha = 1, t) = \frac{m_2(t)}{t}$ supposing $\alpha = 1$. All the curves go downward for $t \gg 1$ to form the lower half of the

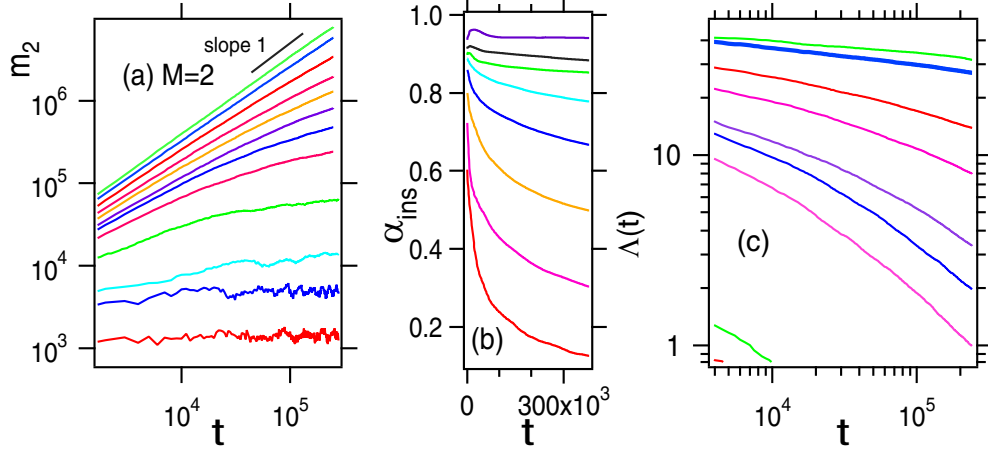


FIG. 12. (a) The double-logarithmic plots of $m_2(t)$ as a function of time for some values of the perturbation strength ϵ increasing from $\epsilon = 0.1$ to $\epsilon = 1.3$ in model A of $M = 2$ with $W = 1$. (b) The instantaneous diffusion index $\alpha_{\text{ins}}(t)$ as a function of time. (c) The double-logarithmic plots of the scaled MSD $\Lambda(\alpha = 1, t) = \frac{m_2(t)}{t}$ as a function of time for some ϵ 's from $\epsilon = 0.1$ to $\epsilon = 1.3$.

precritical trumpet-shaped shown in Figs. 6(c) and 6(f) for $M \geq 3$. All the above results allow us to regard the normal diffusion $m_2(t) \propto t$ as an ultimate limit of the critical subdiffusion for $M = 2$, and $d_f = M = 2$ is just the critical dimension of localization exhibited by model A.

Furthermore, we confirmed that the above features do not change when the random potential $V(n, t)$ is replaced by

$$V(n, t) = V_1(n) + V_2(n)f_\epsilon(t), \quad (25)$$

where $V_1(n)$ and $V_2(n)$ are different random sequences. The same is true if binary random sequences taking $-W$ or W are used for $V_1(n)$ and $V_2(n)$.

VI. DELOCALIZED STATES

In this section, we investigate the characteristics of the delocalized states which emerge for $M \geq 3$ and $\epsilon > \epsilon_c$ in comparison with the stochastic model. Results are compared also with model B with no static random potential.

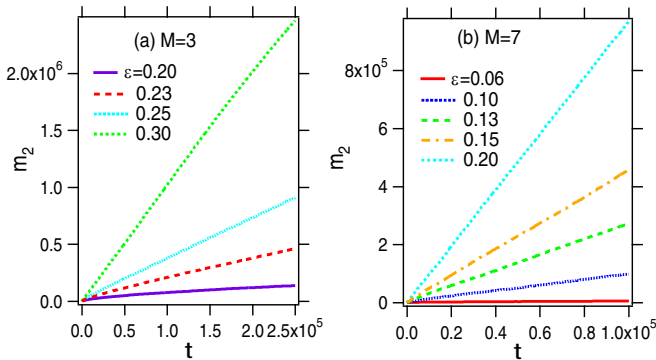


FIG. 13. The $m_2(t)$ as a function of time in model A of (a) $M = 3$ and (b) $M = 7$ with $W = 1$ for some values of the perturbation strength ϵ , increasing from $\epsilon = 0.1$ (bottom) to $\epsilon = 0.2$ (top) for $M = 7$ and from $\epsilon = 0.2$ (bottom) to $\epsilon = 0.3$ (top) for $M = 3$, respectively. Note that the axes are in the real scale.

A. Comparison with stochastic models

We investigate the dependency upon the two parameters W and ϵ in comparison with the D of the stochastic model by Haken and others [11–14].

Typical examples of the $m_2(t)$ for $\epsilon \gg \epsilon_c$ in the cases of $M = 3$ and $M = 7$ are shown in Figs. 13(a) and 13(b), respectively. If ϵ is large enough, it is evident that MSD follows asymptotically the normal diffusion $m_2 = Dt$, which implies that only a finite number of coherent modes plays the same role as the stochastic perturbation.

Indeed, the W dependence of the diffusion coefficient D depicted in Fig. 14 follows the main feature of the stochastically induced diffusion constants regardless of the number of colors $M (\geq 3)$. The dependence changes in the weak regime and strong regime of W as

$$D \propto \begin{cases} W^{-2} & (W \ll 1) \\ W^{-4} & (W \gg 1). \end{cases} \quad (26)$$

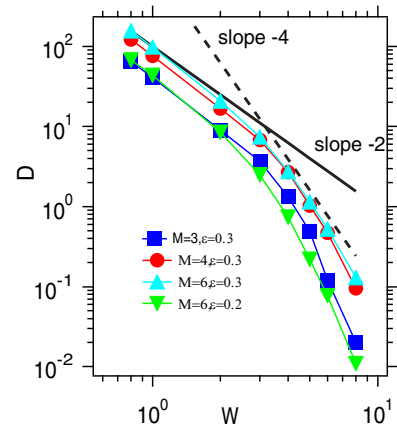


FIG. 14. The diffusion coefficient D of the quantum diffusion as a function of W in model A with $\epsilon = 0.2$ or $\epsilon = 0.3$ of $M = 3, 4, 6$. Note that the axes are in the logarithmic scale. $D \propto W^{-2}$ and $D \propto W^{-4}$ are shown by black solid and black dotted lines, respectively, for reference.

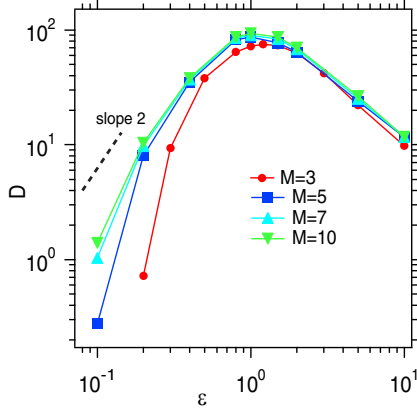


FIG. 15. The diffusion coefficient D as a function of ϵ for model A with $W = 1$ and $M = 3, 5, 7, 10$. Note that the axes are in the logarithmic scale. $D \propto \epsilon^2$ is shown by a black line for reference.

The weak regime result follows Eq. (8) if $W \gg \epsilon$. The strong regime behavior agrees with the result obtained by Moix *et al.* [13] for the stochastic model in the very large limit of W .

Next, we examine the ϵ dependence of D , which is shown in Fig. 15 for some M 's. As a whole, the ϵ dependence almost follows Eq. (8) for all M . [We note that Eq. (8) is valid for small ϵ and W , and it cannot be directly applied to the interpretation of our result.] If ϵ is weak D increases as

$$D \propto \epsilon^2 \quad (27)$$

for $M \gg 1$ in agreement with Eq. (8), and after going over the maximum value at $\epsilon^* \sim O(1)$, it decreases. In particular in the regime $\epsilon > \epsilon^*$, D has no significant M dependence. This fact implies a remarkable feature that the diffusion induced by the coherent perturbation composed of only three incommensurate frequencies mimics the normal diffusion induced by a stochastic perturbation containing an infinite number of colors.

B. Comparison with model B

In the case of $\epsilon = 0$, model B becomes a spatially periodic system without potential part, and the wave packet exactly shows ballistic motion as $m_2(t) \propto t^2$. We consider the MSD for finite ϵ in model B in comparison with model A. Figure 16(a) shows the time evolution of the MSD of model B with $M = 3$ for some values of ϵ . We can see the ballistic growth $m_2(t) \sim t^2$ in the short time regime in all cases. As seen in the M dependence in Fig. 16(b), in model B of $M = 1$, the wave packet localizes. In contrast, for $M \geq 2$ the normal diffusive behavior $m_2 \propto t$, which loses significant M dependence, appears as time proceeds. For more detailed features of the MSD of model B, see Appendix E.

Figure 17 compares the ϵ dependence of the diffusion coefficients D of model B with those of model A. The difference between models A and B is evident in the region $\epsilon_c < \epsilon < \epsilon^*$. In model A, as was stated above, D increases first like ϵ^2 in $\epsilon < \epsilon^*$ and it decreases beyond ϵ^* . But in model B, D decreases monotonously. In the regime $\epsilon < \epsilon^*$, D decreases in contrast to Eq. (27) as

$$D \propto \epsilon^{-2}. \quad (28)$$

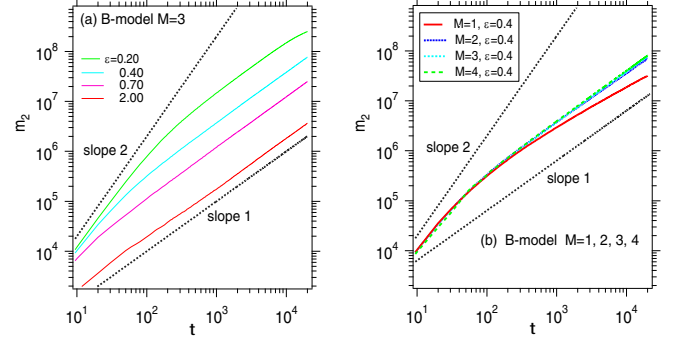


FIG. 16. The double-logarithmic plots of $m_2(t)$ as a function of t in model B with $W = 1$. (a) $M = 3, W = 1$. (b) $M = 1, 2, 3$ and $W = 1$. Note that the axes are in the logarithmic scale. The black dotted line shows $m_2(t) \propto t^1$ for reference.

Beyond ϵ^* , D continues to decrease, which is closely followed by model A. Thus the diffusion processes of the two models become indistinguishable in the region $\epsilon \gg \epsilon^*$ for $M \geq 3$. The above tendency is the same even when we examine the stochastic model by replacing $f_\epsilon(t)$ with $n(t)$. For $\epsilon > \epsilon^*$, the ϵ dependence of the diffusion coefficient D of model SA also approaches that of model SB (see Fig. 22 in Appendix E).

VII. SUMMARY AND DISCUSSION

We investigated systematically the localization-delocalization transition (LDT) of the one-dimensional Anderson model which is dynamically perturbed by polychromatically quasiperiodic oscillations by changing three parameters: the disorder strength W , the perturbation strength ϵ , and the number of colors, M , of the oscillations. The dynamical localization length (LL) was evaluated by the MSD computed by the numerical wave-packet propagation. Although our model consists of $M + 1$ degrees of freedom, we analyzed the numerical results under the hypothesis that

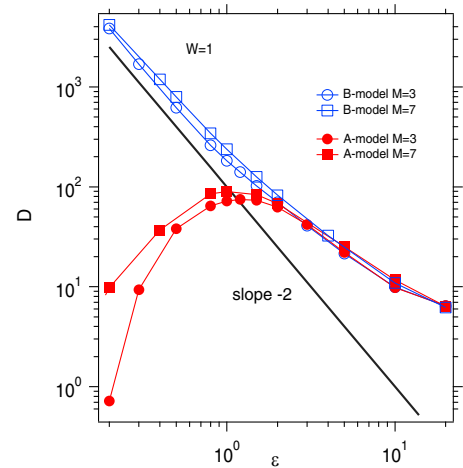


FIG. 17. The diffusion coefficient D of the quantum diffusion as a function of ϵ in models A and B for several M with $W = 1$. The corresponding results for the ballistic model are also provided. Note that the axes are in logarithmic scale. $D \propto \epsilon^{-2}$ is shown by a black line for reference.

TABLE I. Dimensionality of the LDT. For $4 \leq M < \infty$ the result is the same as the case of $M = 3$. The lower lines are a result of the d -dimensional disordered systems by the scaling theory of the localization. Loc, exponential localization; LDT, localization-delocalization transition, Diff, normal diffusion.

M	0	1	2	3	4
This study (model A)	Loc	Loc	Loc	LDT	LDT
This study (model B)	Bali	Loc	Diff	Diff	Diff
Anderson map [20]	Loc	Loc	LDT	LDT	LDT
Standard map [20]	Loc	Loc	LDT	LDT	LDT
d	1	2	3	4	5
Anderson model	Loc	Loc	LDT	LDT	LDT

the effective dimension d_f is M , not $M + 1$, considering the energy conservation. The transition to delocalization is observed for $M = d_f + 1 \geq 3$, and for $M = d_f + 1 \leq 2$ only localization takes place, which is consistent with the d -dimensional Anderson model if d_f is identified with d .

For $M \leq 2$ the LL increases exponentially with respect to ϵ if ϵ is relatively small. On the other hand, the W dependence of the LL is also scaled by the disorder strength W as in the case of the Anderson map (AM).

For $M \geq 3$ the LDT always takes place with increase in the perturbation strength ϵ , and at the critical point ϵ_c the fractional diffusion $\text{MSD} \propto t^\alpha$ ($0 < \alpha < 1$) is observed. The critical diffusion exponent decreases as $\alpha \simeq 2/M$ with M in accordance with the prediction of one-parameter scaling theory (OPST) under the hypothesis $d_f = M$. The numerical results reveal that the critical perturbation strength decreases as $\epsilon_c \propto 1/(M - 2)^{1/2}$ with an increase of M . These properties are different from those of the AM system reported in previous papers [20]. On the other hand, the dimensional dependence of the critical exponent ν of the localization length (LL) roughly estimated by the numerical data was a result qualitatively consistent with those of the polychromatically perturbed AM system with $M - 1$ colors and the LDT in the d -dimensional Anderson model.

Table I summarizes the localization and delocalization phenomena of the random systems, including the case of the random system of the spatial dimension d and the perturbed quantum map systems.

We also studied the delocalized states for $\epsilon > \epsilon_c$. Even though M is not large, the W and ϵ dependence of the diffusion coefficient of the delocalized states mimics those predicted for the stochastically perturbed 1D Anderson model.

As $\epsilon > O(1)$ the characteristics of diffusion of our model approach closely those of model B which contains only the quasi-periodically-oscillating random potential and has no static randomness.

Recently tight-binding models have been implemented by ultracold atoms in the optical lattice [16,17]. If random potential can experimentally be prepared by an optical lattice, for example, by superposing static incommensurate optical standing waves in multiple boundary mirrors, experiments simulating the models discussed in our paper can be implemented under the application of optical harmonic perturbations.

TABLE II. The frequencies S_1 we mainly used are the following: $\omega_1 = (1 + \sqrt{5})/2$, $\omega_2 = 2\pi/\lambda$, $\omega_3 = 2\pi/\lambda^2$, $\omega_4 = \sqrt{3} - 1$, $\omega_5 = \sqrt{2} - 1$, $\omega_6 = \sqrt{13}/2 - 1$, $\omega_7 = \sqrt{11} - 3$, $\omega_8 = \sqrt{10}/2 - 1$, $\omega_9 = 5\sqrt{17} - 20$, and $\omega_{10} = 2\sqrt{19}/2 - 1$, where λ denotes the real root of the cubic equation $x^3 - x - 1 = 0$. We have checked for another set of the frequencies. The whole tendency of the main result in the present paper is not dependent on the choice for the long-time calculation with large system size. S_2 and S_3 are used to get the data of $M = 6$ and $M = 7$ for checking. r_k ($k = 1, \dots, 7$) take uniform random numbers within $[0, 1]$.

ω_M	S_1	S_2	S_3
ω_1	σ	$1 + \sqrt{1/7}$	$1/2 + r_1$
ω_2	ν_1	$1 + \sqrt{2/7}$	$1/2 + r_2$
ω_3	ν_2	$1 + \sqrt{3/7}$	$1/2 + r_3$
ω_4	$\sqrt{3} - 1$	$1 + \sqrt{5/7}$	$1/2 + r_4$
ω_5	$\sqrt{2} - 1$	$1 + \sqrt{7/7}$	$1/2 + r_5$
ω_6	$\sqrt{13}/2 - 1$	$1 + \sqrt{10/7}$	$1/2 + r_6$
ω_7	$\sqrt{11} - 3$	$1 + \sqrt{11/7}$	$1/2 + r_7$
ω_8	$\sqrt{10}/2 - 1$		
ω_9	$5\sqrt{17} - 20$		
ω_{10}	$2\sqrt{19}/2 - 1$		

In the case of a system in which polychromatic perturbation is applied to a three-dimensional disordered system, it is expected that the phenomenon observed will differ greatly depending on the disorder strength W . In the metallic regime of $W < W_c$, the diffusion coefficient of normal diffusion is enhanced by an increase of perturbation strength ϵ , while in the insulating regime of $W \gg W_c$, the LDT occurs at the critical perturbation strength and diffusion is generated, as in the case of the one-dimensional system.

ACKNOWLEDGMENTS

The authors are very grateful to Dr. T. Tsuji and to Koike memorial house for use of the facilities during this study.

APPENDIX A: FREQUENCY SET USED IN THE CALCULATION

Table II shows the sets, S_1, S_2, S_3 , of the frequency set $\{\omega_i\}$. S_1 is mainly used in the text and, as mentioned in the text, is set to be $O(1)$ in the incommensurate as much as possible. The frequency set relatively affects the numerical result compared to the case of the Anderson map system, although the larger the M , the smaller the influence of how to select the frequency. Therefore, in addition to the fundamental frequency set S_1 , we investigated the result in model A with the other frequency sets S_2, S_3 given in Table II. Randomly chosen values are used for S_3 . S_2 was used for numerical calculation by sixth-order symplectic integrator in our previous paper [22].

APPENDIX B: AUTONOMOUS REPRESENTATION OF THE TIME-DEPENDENT SCHRÖDINGER EQUATION (1)

Let the wavefunction describing the whole system composed of the one-dimensional lattice and the M harmonic modes be $|\Psi(t)\rangle$. We introduce the set of the action-angle

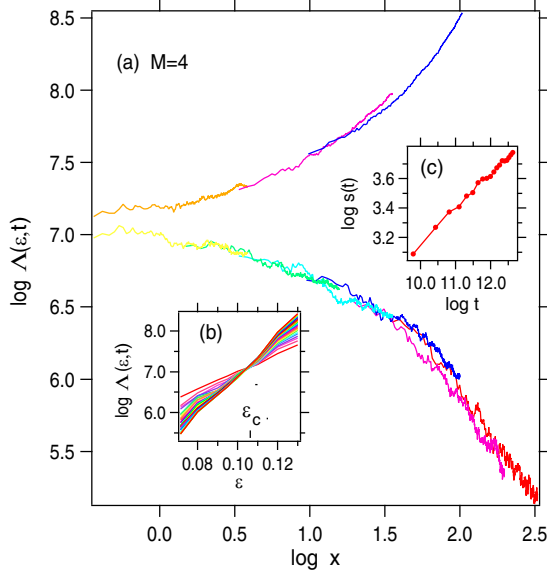


FIG. 18. The results of the critical scaling analysis for model A of $M = 4$ with $W = 1.0$. (a) The scaled MSD $\Lambda(\epsilon, t)$ as a function of $x = \xi_M t^{\alpha/2\nu}$ in logarithmic scale for some values of ϵ , where ξ_M is the localization length as a scaling parameter. (b) The scaled $\Lambda(t)$ with $\alpha = 0.5$ as a function of ϵ for some pickup times. The crossing point is $\epsilon_c \simeq 0.115$. (c) $s(t)$ as a function of t . The critical exponent $\nu \simeq 0.9$ is determined by a scaling relation [Eq. (23)] by the least-squares fit.

operators $(\hat{J}_i, \hat{\phi}_i) := (-i\hbar \frac{\partial}{\partial \phi_i}, \phi_i)$ ($i = 1, 2, \dots, M$) representing the harmonic modes, and let \hat{H}_0 be the part of Hamiltonian in Eq. (1) without the harmonic perturbations (i.e., $\epsilon = 0$) and introduce the Hamiltonian $\hat{h} = \sum_{i=1}^M \omega_i \hat{J}_i$ representing the harmonic modes. The autonomous version of Eq. (1) is written as the evolution equation,

$$i\hbar \frac{\partial |\Psi(t)\rangle}{\partial t} = \hat{H}_{\text{tot}} |\Psi(t)\rangle, \quad (\text{B1})$$

of the whole system with the total Hamiltonian

$$\hat{H}_{\text{tot}} = \hat{H}_0 + \hat{h} + \frac{W\epsilon}{\sqrt{M}} \sum_N v_n |n\rangle \langle n| \sum_{i=1}^M \cos(\phi_i), \quad (\text{B2})$$

where $H_0 = \sum_n (|n+1\rangle \langle n| + |n\rangle \langle n+1|) + W v_n |n\rangle \langle n| = \sum_N E_N |N\rangle \langle N|$ is the unperturbed Hamiltonian, and $|n\rangle$ is the base specifying the site n of the 1D Anderson model. The eigenstate of the action operator, which is angle represented as $\langle \phi_i | J_i \rangle = e^{iJ_i \phi_i / \hbar} / \sqrt{2\pi}$ with the action eigenvalue $J_i = n_i \hbar$, is written as $|n_i\rangle$, and we let the eigenstate of the isolated one-dimensional lattice H_0 be $|N\rangle$ with eigenvalue E_N : $H_0 |N\rangle = E_N |N\rangle$. By decomposing the quantum state of the total system as $|\Psi(t)\rangle = \sum_{N, \{n_i\}} \Psi(N, \{n_i\}) |N, \{n_i\}\rangle$, Eq. (B2) is rewritten by Eq. (1).

Let $\hat{U}_{\text{tot}} = \exp\{-i\hat{H}_{\text{tot}} t / \hbar\}$ be the unitary evolution operator of the total system, and introduce the new operator \hat{U} by $\hat{U}_{\text{tot}} = e^{-i\hat{h}t/\hbar} \hat{U}$. Then the evolution equation

$$i\hbar \frac{\partial \hat{U}}{\partial t} = \left[H_0 + \frac{W\epsilon}{\sqrt{M}} \sum_n v_n |n\rangle \langle n| \sum_{i=1}^M \cos(\omega_i t + \phi_i) \right] \hat{U}$$

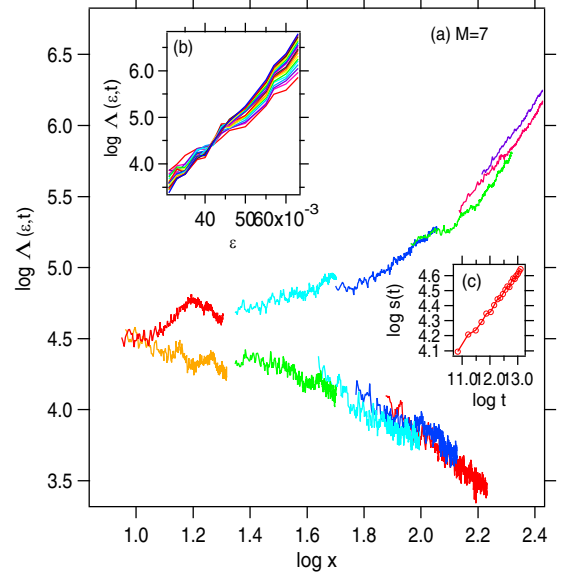


FIG. 19. The results of the critical scaling analysis for model A of $M = 7$ with $W = 1.0$. (a) The scaled MSD $\Lambda(\epsilon, t)$ as a function of $x = \xi_M(\epsilon) t^{\alpha/2\nu}$ in logarithmic scale for some values of ϵ , where ξ_M is the localization length as a scaling parameter. (b) The scaled $\Lambda(t)$ with $\alpha = 0.28$ as a function of ϵ for some pickup times. The crossing point is $\epsilon_c \simeq 0.042$. (c) $s(t)$ as a function of t . The critical exponent $\nu \simeq 0.52$ is determined by a scaling relation [Eq. (23)] by the least-squares fit.

is immediately obtained, which is equivalent to Eq. (1) if the phase eigenstate $|\phi_1\rangle, |\phi_2\rangle, \dots, |\phi_M\rangle$ is supposed at $t = 0$. The identity

$$e^{i\hat{J}_i \omega t / \hbar} e^{-iK \cos \phi / \hbar} e^{-i\hat{J}_i \omega t / \hbar} = e^{-iK \cos(\phi + \omega t) / \hbar} \quad (\text{B3})$$

is used.

APPENDIX C: AN ALTERNATIVE REPRESENTATION OF EQ. (4)

Equation (B2) allows us to introduce an alternative representation of Eq. (4) based upon the quantum state of a single lattice site dressed with harmonic modes interacting

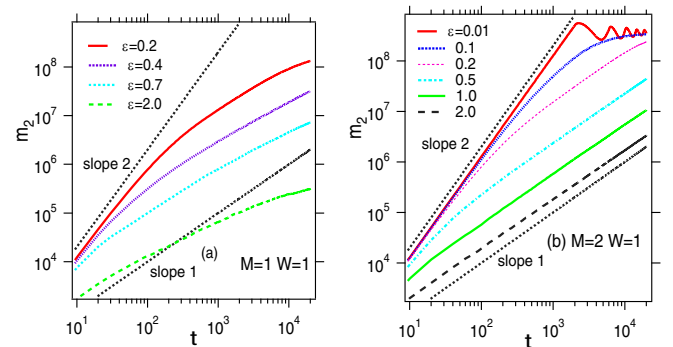


FIG. 20. The double-logarithmic plots of $m_2(t)$ as a function of t for different values of ϵ in model B with $W = 1$: (a) $M = 1$ and (b) $M = 2$. Black dotted and thick lines show $m_2(t) \propto t^2$ and $m_2(t) \propto t^1$, respectively, for reference.

with it. We demonstrate the $M = 1$ case. Let us focus on the part of Hamiltonian (B2), from which the transfer term $\sum_n(|n+1\rangle\langle n| + |n\rangle\langle n+1|)$ is neglected,

$$\hat{H}^{(n)} = \omega\hat{J} + Wv_n(1 + \epsilon \cos \phi)|n\rangle\langle n|, \quad (\text{C1})$$

which represents the n th site interacting with the harmonic mode. We set $\omega_1 = \omega$. Suppose its eigenstates of the form $|n, K\rangle = |n\rangle|K\rangle_n$, satisfying $\hat{H}_n|n, K\rangle = E_{n,K}|n, K\rangle$, where K is the new quantum number associate with the harmonic mode to be introduced later. One can readily find that the ϕ representation $\langle \phi|K\rangle_n := u_{K,n}(\phi)$ of $|K\rangle_n$ satisfies the simple equation

$$i\omega \frac{\partial u_{K,n}}{\partial \phi} = [Wv_n(1 + \epsilon \cos \phi) - E_{n,K}]u_{K,n}, \quad (\text{C2})$$

which leads to

$$u_{K,n}(\phi) = \frac{1}{\sqrt{2\pi}} \exp \left[i \frac{(E_{n,K} - Wv_n)\phi - Wv_n\epsilon \sin \phi}{\hbar\omega} \right], \quad (\text{C3})$$

where the quantization condition $E_{n,K} - Wv_n = K\omega\hbar$ (K is an arbitrary integer) is required for the 2π periodicity of $u_{K,n}(\phi)$. Using the new basis $|n, K\rangle = |n\rangle|K\rangle_n$ we expand the wavefunction as $\Psi(t) = \sum_{n,K} \Phi(n, K)|n, K\rangle$, and the Schrödinger equation in Eqs. (B1) and (B2) is rewritten into the following form, instead of Eq. (4) with $M = 1$:

$$i\hbar \frac{d\Phi(n, K)}{dt} = (K\omega\hbar + Wv_n)\Phi(n, K) + \sum_{K'} [T_{K-K'}^{n, n+1} \times \Phi(n+1, K') + T_{K'-K}^{n, n-1} \Phi(n-1, K')]. \quad (\text{C4})$$

Then the effective position-dependent hopping is given as

$$T_{K-K'}^{n, n'} := {}_n \langle K|K'\rangle_{n'} = J_{K-K'} \left(\frac{\epsilon W(v_n - v_{n'})}{\hbar\omega} \right), \quad (\text{C5})$$

where $J_n(x)$ is the first kind of Bessel function. We can see that the monochromatic perturbation combined with the randomness is completely incorporated into the hopping terms. The amplitude $\Phi(n, K)$ at each lattice site (n, K) is connected to those at the sites $(n \pm 1, K - K')$. It follows that for $\epsilon W/\hbar\omega \ll 1$ the hopping coefficients decay along the K direction, and the system becomes a quasi-1D tight-binding model because $J_n(x) \sim \frac{x^n}{2^n n!}$ as $n \rightarrow \infty$.

Similarly, in the case of model B of $M = 1$, the model can be converted into a tight-binding model without the on-site randomness and with hopping randomness.

APPENDIX D: RESULT OF FINITE-TIME CRITICAL SCALING ANALYSIS

Figures 18 and 19 display the results of the finite-time scaling analysis for model A of $M = 4$ and $M = 7$, respectively. As a result, the OPST is well established for the LDT regardless of the number of colors, M , and the disorder strength W .

APPENDIX E: NORMAL DIFFUSION OF MODEL B

Unlike model A, in model B the system starts with the ballistic motion $m_2 \propto t^2$, and the motion gradually changes as

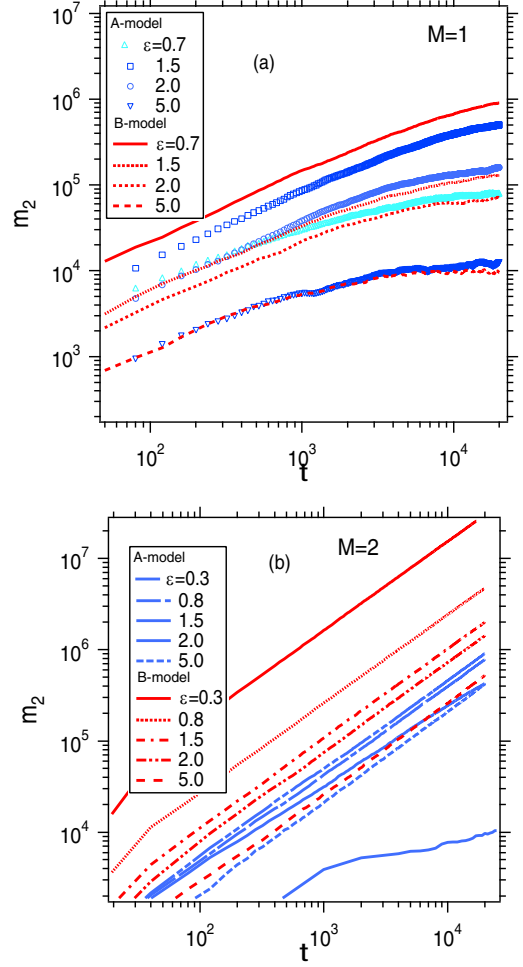


FIG. 21. The double-logarithmic plots of $m_2(t)$ as a function of t for different values of ϵ in models A and B with $W = 1$: (a) $M = 1$ and (b) $M = 2$.

the perturbation becomes effective. The time dependence of the MSD of $M = 1$ and $M = 2$ is shown in Fig. 20. As shown in Fig. 20(a), in the case of $M = 1$, irrespective of the magnitude of ϵ , the double-logarithmic plots of $m_2(t)$ tell that its instantaneous slope $\alpha_{\text{inst}}(t)$ finally decreases gradually below $\alpha = 1$, and we cannot find any sign that $\alpha_{\text{inst}}(t)$ converges to a nonzero value. We, therefore, conjecture that delocalization does not occur for $M = 1$.

On the other hand, in the case of $M = 2$, as shown in Fig. 20(b), the time domain in which the ballistic motion is taking place is reduced by increasing ϵ , and normal diffusion, $m_2(t) \simeq Dt$, finally appears. (Due to the system size of numerical calculation, it tends to be saturated when it reaches the boundary.) We conjecture that, no matter how small the magnitude of ϵ may be, the ballistic motion $m_2(t) \simeq t^2$ changes into diffusive motion $m_2(t) \simeq t^1$ in a long-time limit, if the system size is infinite. Similar behavior can be expected also for $M \geq 3$, and there is no LDT.

Figure 21 shows a comparison of $m_2(t)$ for some ϵ 's in models A and B. Figure 21(a) is for $M = 1$. The MSD of model A increases as ϵ increases, but it decreases for $\epsilon > \epsilon^*$,

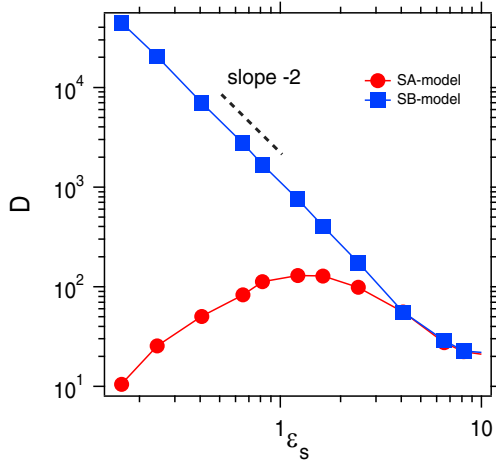


FIG. 22. The diffusion coefficient D of the quantum diffusion as a function of ϵ in models SA and SB with $W = 2.0$. Note that the axes are in logarithmic scale and $\epsilon_s^* \simeq 1.15$ for $W = 2$. $D \propto \epsilon_s^{-2}$ is shown by black dotted lines as a reference.

where $\epsilon^* \sim 1$ is the characteristic value given in the text. At $\epsilon \gg \epsilon^*$, it can be seen that the $m_2(t)$ of model A approaches the result of model B, and it overlaps for $\epsilon = 5$ with that of model B. Both cases become localized. As mentioned in the main text, it can be said that it is an asymptotic transition from model A to model B as ϵ increases. Figure 21(b) is the result for $M = 2$. For $\epsilon = 5.0$ both cases show normal diffusive behavior for $\epsilon \gg 1$.

Moreover, as can be seen in the localized case of $\epsilon = 0.7$ and $\epsilon = 2.0$ in model A of $M = 1$ in Fig. 21(a), the time dependence of $m_2(t)$ intersects. It follows that the two types of regions, $\epsilon < \epsilon^*$ and $\epsilon > \epsilon^*$, do not follow the same scaling curve towards localization even if the localization length is the same

Figure 22 shows a comparison of the ϵ_s dependence of the diffusion coefficient in models SA and SB. It can be seen that model SA has a peak around $\epsilon_s^* \simeq 1.15$ and $D(\epsilon_s)$ gradually approaches that of model SB for $\epsilon_s \gg \epsilon_s^*$. This tendency is the same as the relationship between model A and model B.

- [1] P. W. Anderson, *Phys. Rev.* **109**, 1492 (1958).
- [2] K. Ishii, *Prog. Theor. Phys. Suppl.* **53**, 77 (1973).
- [3] L. M. Lifshiz, S. A. Gredeskul, and L. A. Pastur, *Introduction to the Theory of Disordered Systems* (Wiley, New York, 1988).
- [4] *50 Years of Anderson Localization*, edited by E. Abrahams (World Scientific, Singapore, 2010).
- [5] P. Markos, *Acta Phys. Slovaca* **56**, 561 (2006).
- [6] A. M. Garcia-Garcia and E. Cuevas, *Phys. Rev. B* **75**, 174203 (2007).
- [7] Y. Ueoka and K. Slevin, *J. Phys. Soc. Jpn.* **83**, 084711 (2014).
- [8] E. Tarquini, G. Biroli, and M. Tarzia, *Phys. Rev. B* **95**, 094204 (2017).
- [9] D. Vollhardt and P. Wölfle, *Phys. Rev. Lett.* **45**, 842 (1980); *Phys. Rev. B* **22**, 4666 (1980); *Phys. Rev. Lett.* **48**, 699 (1982).
- [10] P. Wölfle and D. Vollhardt, *Int. J. Mod. Phys B* **24**, 1526 (2010).
- [11] H. Haken and P. Reineker, *Z. Phys.* **249**, 253 (1972); H. Haken and G. Strobl, *ibid.* **262**, 135 (1973).
- [12] M. A. Palenberg, R. J. Silbey, and W. Pfluegl, *Phys. Rev. B* **62**, 3744 (2000).
- [13] J. M. Moix, M. Khasin, and J. Cao, *New J. Phys.* **15**, 085010 (2013).
- [14] S. Gopalakrishnan, K. R. Islam, and M. Knap, *Phys. Rev. Lett.* **119**, 046601 (2017).
- [15] G. Casati, I. Guarneri, and D. L. Shepelyansky, *Phys. Rev. Lett.* **62**, 345 (1989).
- [16] M. Lopez, J. F. Clement, P. Szczygiser, J. C. Garreau, and D. Delande, *Phys. Rev. Lett.* **108**, 095701 (2012).
- [17] M. Lopez, J.-F. Clement, G. Lemarie, D. Delande, P. Szczygiser, and J. C. Garreau, *New J. Phys.* **15**, 065013 (2013).
- [18] H. S. Yamada, F. Matsui, and K. S. Ikeda, *Phys. Rev. E* **92**, 062908 (2015).
- [19] H. S. Yamada, F. Matsui, and K. S. Ikeda, *Phys. Rev. E* **97**, 012210 (2018).
- [20] H. S. Yamada and K. S. Ikeda, *Phys. Rev. E* **101**, 032210 (2020).
- [21] H. Yamada and K. S. Ikeda, *Phys. Lett. A* **248**, 179 (1998).
- [22] H. Yamada and K. S. Ikeda, *Phys. Rev. E* **59**, 5214 (1999).
- [23] M. Holthaus, G. H. Ristow, and D. W. Hone, *Phys. Rev. Lett.* **75**, 3914 (1995).
- [24] D. F. Martinez and R. A. Molina, *Phys. Rev. B* **73**, 073104 (2006).
- [25] H. Hatami, C. Danieli, J. D. Bodyfelt, and S. Flach, *Phys. Rev. E* **93**, 062205 (2016).
- [26] J. Bourgain and W. Wang, *Commun. Math. Phys.* **248**, 429 (2004).
- [27] H. S. Yamada and K. S. Ikeda, *Phys. Rev. E* **103**, L040202 (2021).
- [28] M. C. Gutzwiller, *Chaos in Classical and Quantum Mechanics* (Springer-Verlag, Berlin, 1991).
- [29] F. Borgonovi and D. L. Shepelyansky, *Physica D* **109**, 24 (1997).
- [30] C. Neill *et al.*, *Nat. Phys.* **12**, 1037 (2016).
- [31] S. Notarnicola, F. Iemini, D. Rossini, R. Fazio, A. Silva, and A. Russomanno, *Phys. Rev. E* **97**, 022202 (2018).
- [32] A. Piga, M. Lewenstein, and J. Q. Quach, *Phys. Rev. E* **99**, 032213 (2019).
- [33] K. Ikeda, *Ann. Phys.* **227**, 1 (1993).